

# RSC Advances



This is an *Accepted Manuscript*, which has been through the Royal Society of Chemistry peer review process and has been accepted for publication.

*Accepted Manuscripts* are published online shortly after acceptance, before technical editing, formatting and proof reading. Using this free service, authors can make their results available to the community, in citable form, before we publish the edited article. This *Accepted Manuscript* will be replaced by the edited, formatted and paginated article as soon as this is available.

You can find more information about *Accepted Manuscripts* in the [Information for Authors](#).

Please note that technical editing may introduce minor changes to the text and/or graphics, which may alter content. The journal's standard [Terms & Conditions](#) and the [Ethical guidelines](#) still apply. In no event shall the Royal Society of Chemistry be held responsible for any errors or omissions in this *Accepted Manuscript* or any consequences arising from the use of any information it contains.

**Effect of Ru substitution on the physical properties of  
 $\text{La}_{0.6}\text{Pr}_{0.1}\text{Sr}_{0.3}\text{Mn}_{1-x}\text{Ru}_x\text{O}_3$  ( $x=0.00, 0.05$  and  $0.15$ ) perovskites**

N. Zaidi<sup>a</sup>, S. Mnefgui<sup>a</sup>, J. Dhahri<sup>a</sup> and E.K. Hlil<sup>b</sup>

<sup>a</sup> *Laboratoire de la matière condensée et des nanosciences, Université de Monastir, 5019, Tunisia*

<sup>b</sup> *Institut Néel, CNRS et Université Joseph Fourier, B.P. 166, 38042 Grenoble, France*

**Abstract**

Morphology, magnetic, and magnetocaloric properties of  $\text{La}_{0.6}\text{Pr}_{0.1}\text{Sr}_{0.3}\text{Mn}_{1-x}\text{Ru}_x\text{O}_3$  ( $x=0.00, 0.05$  and  $0.15$ ) were experimentally investigated. Solid-state reaction method was used in the preparation of the samples. The microstructure of the samples was determined by scanning electron microscopy SEM. Field-cooled (FC) and zero-field-cooled (ZFC) thermomagnetic curves measured at low field and low temperatures exhibit a cluster spin state. A sensitive response to substituting Ru for Mn is observed in the magnetic and magnetocaloric properties. We found that Ru doping is not powerful enough to reduce Curie temperature  $T_C$ , however, it brings about cluster glass behaviors. A magneto-caloric effect has been calculated in terms of isothermal magnetic entropy change. The maximum entropy change  $|\Delta S_M^{\max}|$  reaches the highest values of 3.32 J/KgK, 3.11 J/KgK and 2.57 J/KgK in a magnetic field. However, the relative cooling power decreases with Ru content from 227.44J/Kg to 214.14 J/Kg and then to 188.68 J/Kg for  $x=0.00, 0.05$  and  $0.15$  compositions respectively.

**Key words:** Morphology; Magnetization; Magnetocaloric effect ; Manganites

**Corresponding author email address:** [zaidinadia77@yahoo.com](mailto:zaidinadia77@yahoo.com)

**Tel:** (+216) 97 54 31 31

## 1. Introduction

The hole-doped mixed valence perovskite manganites of  $D_{1-x}A_xMn_{1-y}B_yO_3$  type (where  $D$  is a trivalent rare earth,  $A$  is a divalent alkali earth and  $B$  is the transition metals) have attracted considerable attention during the last decade. In these perovskite compounds, the interplay between magnetism, charge ordering and electronic transport have been studied in detail [1-4]. In particular, the metal-insulator transition near the Curie temperature in this type of materials has been interpreted in terms of the double exchange (DE) model. Other mechanisms have also provided valuable insights into the colossal magnetoresistance (CMR) phenomenon in manganites, such as the antiferromagnetic super-exchange, Jahn-Teller effects, orbital and charge ordering [5,6]. Other researches focused on perovskite manganites with a general formula  $D_{1-x}A_xMnO_3$  after observing large magnetocaloric effects (MCE) in these compounds [7-10]. Currently, magnetocaloric effect (MCE) offers an alternative technology in refrigeration, with an enhanced efficiency but without environmental hazards [11-14]. The key in using magnetic refrigeration at room temperature is to seek the proper refrigerant materials which can produce a large entropy variation when it goes through a magnetization-demagnetization process. In terms of the crucial role of Mn site, it would be interesting and worthwhile to study the effects of Mn-site element substitution, which may provide clues for exploring novel MCE materials and concerning the mechanism of MCE. Within this framework, the effect of substituting trivalent ions such as Fe, Ni and Sc for  $Mn^{3+}$  ions in the  $B$  site on the ferromagnetic properties of these manganites has been studied [15-18]. It was experimentally found that any modification on the exchange interaction causes the pair-breaking effect associated with a drastic reduction in Curie temperature  $T_C$ . However, differently from the common ionic substitution, Ru doping in manganites has a peculiar effect and is attracting more attention. A slight substitution of Ru for Mn ions favors the formation of the ferromagnetic metal (FMM) states [19-21]. Additionally, it was reported that as high as 30 at. % of Ru can be added into the Mn sites in  $La_{0.7}Sr_{0.3}MnO_3$ , with no change in the crystal structure and a weak effect on the reduction of  $T_C$  [22]. It is argued that Ru has a more delocalized  $4f$  orbital with itinerant  $t_{2g}$  electrons that facilitate the exchanges coupling interaction. That is to say that, Ru could make a magnetic pair with Mn to form the Mn-O-Mn network, thus favoring the DE-mediated transport mechanism. Enhanced magnetic and metal-

insulator transition temperature in Ru-doped layered manganites  $La_{1.2}Ca_{1.8}Mn_{2-x}Ru_xO_7$  have been reported [23-30]. It is known from the literature that mixed valence of  $Ru^{3+}/Ru^{4+}$  appears in the lower-doping region ( $0 \leq 0.5$ ) while an additional mixed valence of  $Ru^{4+}/Ru^{5+}$  appears in the high-doping region ( $0 \geq 0.5$ ) [31].

$La_{0.6}Pr_{0.1}Sr_{0.3}MnO_3$  is one of the perovskite compounds which possess rich physical properties but a relatively high Curie temperature ( $T_C=360K$ ) [32]. Potential applications, particularly magnetic refrigeration (MR) require a transition temperature  $T_C$  close to room temperature. This can be achieved by an appropriate amount of oxygen stoichiometry or by the substitution of **Mn** by a non-magnetic or magnetic cation. So, to decrease the critical temperature of the parent compound  $La_{0.6}Pr_{0.1}Sr_{0.3}MnO_3$ , we made a substitution of Ruthenium (Ru) for manganese (Mn) by. Then, we investigated the effect of this substitution on the physical properties of  $La_{0.6}Pr_{0.1}Sr_{0.3}MnO_3$ .

## 2. Experimental details

Polycrystalline samples of  $La_{0.6}Pr_{0.1}Sr_{0.3}Mn_{1-x}Ru_xO_3$  series with ( $x=0.00, 0.05$  and  $0.15$ ) were prepared by conventional solid state ceramic processing. High purity (99.99 %) starting compounds  $La_2O_3$ ,  $Pr_6O_{11}$ ,  $SrCO_3$ ,  $MnO_2$  and  $RuO_2$  were taken in stoichiometric proportions. Care was taken to remove moisture before weighing by preheating the precursors at 873 K for 12 h. The mixtures were heated in air at 1073 K for 24 h to achieve decarbonization. After grinding, they were heated at 1373K for 48 h and grind again to ensure homogeneity. Intermediate cooling and mechanical grinding steps were repeated in order to get an accurate homogenization and complete reaction. The powders were pressed into pellets and sintered at 1673 K for 72 h under an Ar/H<sub>2</sub> (5%) atmosphere with several intermediate grinding and repelling. Finally, these pellets were quenched to room temperature [33]. “Magnetizations ( $M$ ) vs. temperature ( $T$ ) were measured using BS1 and BS2 magnetometers developed in Louis Néel Laboratory of Grenoble. BS1 (300-900 K) and BS2 (1.5-300 K) magnetometers are used respectively for magnetic measurements at high and low temperatures equipped with a super conducting coil [34]. These two instruments are automated by a computer system that allows the registration of digital data for each successive measurement. Magnetization isotherms were measured in the range of 0–

5 T and with a temperature interval of 3 K in the vicinity of Curie temperature ( $T_C$ ). These isothermals were corrected by a demagnetization factor  $D$  that was determined by a standard procedure from low-field dc magnetization measurement at low temperatures ( $H=H_{app}-DM$ ). Finally, the magnetocaloric effect (MCE) was characterized by an isothermal change of the magnetic entropy and the adiabatic change of temperature.

### 3. Results and discussions

#### 3.1. morphological characterization

In order to check the existence of all the elements in the LPSMRO (0.00, 0.05 and 0.15) compounds, an energy dispersive X-Ray analysis was performed. An example of EDX spectra is represented in **Fig.1** for  $x=0.05$ . This spectrum reveals the presence of all elements (**La, Pr, Sr, Mn, Ru** and **O**), which confirms that there is no loss of any integrated element during sintering. The SEM micrographs are given in the inset of this figure for  $x = 0.05$ . We can see that the grains exhibit spheroid-like shapes and a good connectivity between each other. This facilitates the intrinsic behaviors, because good current percolation between grains and the opening up of conduction channels do not block the ordering of the Mn spins.

#### 3.2. Magnetic behaviors

**Fig.2. (a)** shows the temperature dependence of the zero field-cooled (ZFC) and field-cooled (FC) magnetization for LPSMRO. As can be seen, all the LPSMRO samples undergo a transition from a ferromagnetic to a paramagnetic phase. It is clear that the 'FC' curves do not coincide with the 'ZFC' curves below  $T_C$ . But the curves 'FC' and 'ZCF' curves have a common part for the high temperature, wherein the variation of magnetization with temperature is reversible and superposed. At low temperature, the behavior is irreversible with a divergence between 'ZFC' and 'FC'. The magnetic moment decreases gradually. Such irreversibility in the M-T data for the FC and 'ZFC' measurements was observed in several manganite systems and it was suggested that this irreversibility is possibly due to the canted nature of the spins or to the random freezing of spins [35]. This can be clearly seen at at low temperature for  $x=0.15$ , which is generally related to a spin-glass or cluster-glass state. The discrepancy between 'ZFC' curve and 'FC' curve becomes proportionally larger with the doped content of Ru. It is found that the Curie temperature  $T_C$  decreases with

increasing  $x$ . The variation of  $T_C$  versus Ru concentration is tabulated in **Table. 1**. One can note that  $T_C$  decreases slowly when Ru content is increased. The abnormal evolution of  $T_C$  indicates that the Ru ionic substitution reduces systematically ferromagnetism. The Curie temperature  $T_C$  determined by linearly extrapolating the temperature dependence of magnetic susceptibility  $1/\chi$  in the paramagnetic state is shown in the inset of **Fig.2. (a)**, which obeys the Curie-Weiss law,  $1/\chi = (T - T_C)/C$  above  $T_C$ . From the obtained Curie constants ( $C$ ), we get the effective moment  $P_{eff}^{exp} = 5.76, 5.45$  and  $4.91 \mu_B$  for  $x=0.00, 0.05$  and  $0.15$ , respectively.

The calculated effective paramagnetic moment per formula can be written as:

$$\mu_{eff}^{th} = \sqrt{n_{Mn^{3+}} [\mu_{eff}^{th}(Mn^{3+})]^2 + n_{Mn^{4+}} [\mu_{eff}^{th}(Mn^{4+})]^2 + [0.1 \mu_{eff}^{th}(Pr^{3+})]^2 + n_{Ru^{3+}} [\mu_{eff}^{th}(Ru^{3+})]^2 + n_{Ru^{4+}} [\mu_{eff}^{th}(Ru^{4+})]^2}$$

,with  $\mu_{eff}^{th}(Mn^{3+}) = 4.9 \mu_B$ ,  $\mu_{eff}^{th}(Mn^{4+}) = 3.87 \mu_B$ ,  $\mu_{eff}^{th}(Pr^{3+}) = 3.58 \mu_B$  [36]

$\mu_{eff}^{th}(Ru^{3+}) = 1.73 \mu_B$  [37]  $\mu_{eff}^{th}(Ru^{4+}) = 2.83 \mu_B$  [38]. The values of  $P_{eff}^{th}$  are 4.751,

4.66 and 4.47 for  $x=0.00, 0.05$  and  $0.15$ , respectively (**Table.2**). The difference between the effective magnetic moments measured and the theoretical values is possibly due to the possible orbital-charge fluctuations in contrast to charge-orbital ordering in the parent compound  $La_{0.6}Pr_{0.1}Sr_{0.3}MnO_3$ .

The field dependence of magnetization at 5K is plotted in the inset of **Fig.2. (b)** in magnetic fields strengths of  $\pm 10T$  to complement the FC versus  $T$  data. The magnetization of all the samples nearly saturates above 1.5 T. On increasing Ru doping, the saturation magnetization ( $M_s$ ) decreases. The hysteresis loops of  $x=0.00$  and  $x=0.15$  samples are plotted at temperature 5K in **Fig.2. (b)**. The hysteresis in the  $M-\mu_0H$  curve, along with the saturation, clearly confirms that we have a ferromagnetic state at low temperatures. It can be clearly seen that both the coercive field ( $\mu_0H_c$ ) and the remanence magnetization ( $M_r$ ) increase systematically with the increases of Ru doping. The coercive field increased by more than an order of magnitude from  $2.610^{-3}$  T for the undoped ( $x=0.00$ ) sample to nearly  $2.310^{-2}$  T for  $x=0.15$  Ru doped sample. Similarly, the Ru doping resulted in a large change of  $M_r$ , by as much as a factor of 4 (**Table 2**).

**Fig.3** shows the variation of remanence magnetization ( $M_r$ ) and saturation magnetization ( $M_s$ ) with  $Ru^{3+}$  substitution. The force required for demagnetization of

a sample is termed as remanence magnetization and is one of the important parameters to be considered in recording media industry. Remanence is a structure sensitive parameter. For the present system the values of remanence varied in the range of 4.60-18.20 emu/g. The remanence ratio  $R=Mr/Ms$  is a characteristic parameter of the material. It is an indication of the ease with which the direction of magnetization reorients to the nearest easy axis of magnetization direction after the magnetic field is removed. Within this framework, it is desirable to have higher remanence ratio for magnetic recording and memory devices [39]. The values of R in the present case varied for one magnitude of order and the values found are 0.054, 0.071 and 0.240 for  $x=0.00$ , 0.05 and 0.15 respectively. The values show an increasing trend with  $Ru^{3+}$  substitution.

Furthermore, to better understand the effect of the substitution of Ru for Mn at low temperature, we calculated the values of saturation magnetic moment at  $T=5K$  considering the total spins of  $Mn^{3+}$ ,  $Mn^{4+}$ ,  $Pr^{3+}$ ,  $Ru^{3+}$  and  $Ru^{4+}$  ions ( $Mn_{SatMn^{3+}} = 4\mu_B(t_{2g}^3 eg^1)$ ,  $M_{SatMn^{4+}} = 3\mu_B(t_{2g}^3 e_g^0)$ ,  $M_{satPr^{3+}} = 2\mu_B$ ,  $M_{SatRu^{3+}} = 3\mu_B(t_{2g}^5 state)$ ,  $M_{SatRu^{4+}} = 2\mu_B(Low-spin t_{2g}^4 state)$ ). The spontaneous magnetizations of the  $La_{0.6}^{3+} Pr_{0.1}^{3+} Sr_{0.3}^{2+} (Mn_{1-x} Ru_x)^{3+} (Mn_{1-x} Ru_x)^{4+} O_3$  compounds are expressed as follows:

$$M_{Sat}(cal) = (M_{SatPr^{3+}})(n_{Pr^{3+}}) + (M_{SatMn^{3+}})(n_{Mn^{3+}}) + (M_{SatMn^{4+}})(n_{Mn^{4+}}) + (M_{SatRu^{3+}})(n_{Ru^{3+}})$$

where  $n_{Mn^{3+}}$ ,  $n_{Mn^{4+}}$ ,  $n_{Pr^{3+}}$  and  $n_{Ru^{3+}}$  are the contents of  $Mn^{3+}$ ,  $Mn^{4+}$ ,  $Pr^{3+}$  and  $Ru^{3+}$  ions respectively and  $\mu_B$  is Bohr magneton. The measured spontaneous magnetizations at  $T=5K$  for  $x = 0.00$ , 0.05 and 0.15 compounds are found to be about 3.61  $\mu_B$ , 3.22  $\mu_B$  and 2.45  $\mu_B$  respectively, while the calculated values for full spin alignment are 3.9  $\mu_B$ , 3.64  $\mu_B$  and 3.191  $\mu_B$ , respectively. The spontaneous magnetization decreases with increasing Ru content. The difference between measured and calculated values especially for  $x=0.15$  should be explained by spin canted state at low temperature [40].

In Fig. 4, we show magnetization isotherms,  $M(\mu_0H)$ , for  $x=0.00$  and  $x=0.15$  samples taken over a certain temperature range around their respective Curie temperatures. The data were taken at 5K intervals close to  $T_C$  and away from  $T_C$ . We found a soft

ferromagnetic behavior at all temperatures in Ru-doped compounds. The same result is shown during Fe doping at Mn site in the same parent compound [40]. Banerjee [41] suggested an experimental criterion which allows the determination of the nature of the magnetic transition (first or second order). It consists in observing the slope of the isotherms plots  $M^2$  versus  $\mu_0 H/M$ . Applying a regular approach, the straight line was constructed simply by extrapolating the high magnetization parts of the curves for each studied temperature. A positive or negative slope indicates a second or a first order transition, respectively. **Fig.5 (a. b)** shows the isotherm plots  $M^2$  versus  $\mu_0 H/M$  above and below  $T_C$  for  $x=0.00$  and  $x=0.15$  samples, respectively. These samples show positive slopes in the complete  $M^2$  range, indicating that the system exhibits a second-order ferromagnetic to paramagnetic phase transition.

### 3.3. Magnetocaloric behaviors

The magnetocaloric effect is an intrinsic property of magnetic materials. It is the response of the material to the application or removal of magnetic field, which is maximized when the material is near its magnetic ordering temperature (Curie temperature  $T_C$ ).

From Maxwell's thermodynamic equation, the magnetic entropy change as the field is varied from  $\mu_0 H = 0$  to  $\mu_0 H = \mu_0 H_{\max}$ . Can be written as:

$$\Delta S_M = \int_0^{\mu_0 H_{\max}} \left( \frac{\partial M}{\partial T} \right)_{\mu_0 H} d\mu_0 H \quad (1)$$

The numerical evaluation of this integral can be approximated to give

$$\Delta S_M = \sum [(M_i(T_i, \mu_0 H) - M_{i+1}(T_{i+1}, \mu_0 H)) / (T_i - T_{i+1})] \Delta \mu_0 H \quad (2)$$

Where  $M_i$  and  $M_{i+1}$  are the magnetization values measured at temperatures  $T_i$  and  $T_{i+1}$ , respectively and  $\Delta \mu_0 H$  represents the field variation from  $\mu_0 H = 0$  until  $\mu_0 H_{\max}$ .

The  $-\Delta S_M$  values for different  $\Delta \mu_0 H$  as a function of temperature are presented in **Fig.6** determined under an applied magnetic field up to 5T. The  $-\Delta S_M$  is positive in the entire temperature range for all the samples. The magnetic entropy for  $\Delta \mu_0 H = 5T$  increases with lowering temperature for  $T \ll T_C$ , others goes through a maximum around  $T_C$  and then decreases for  $T \gg T_C$ . The magnitude of the peak increases with

increasing the value of  $\Delta_{\mu_0}H$  for each composition but the peak position is nearly unaffected because of the second order nature of the ferromagnetic transition in these compounds. Furthermore, the value of the peak decreases with increasing Ru content around  $T_C$  from  $-\Delta S_M = 3.32$  J/Kg K for  $x=0.00$  to  $2.57$  J/Kg K for  $x=0.15$ . It should be noted that  $|\Delta S_M^{\max}|$  values found in this study are relatively the same as that observed by R. Cherif et al for  $x=0.00$  [40]. For comparison, we listed in **Table.2** the data of various magnetic materials that could be used as magnetic refrigerants. Although the values of  $|\Delta S_M^{\max}|$  are smaller than the most conspicuous MC material  $\text{La}(\text{Fe}_{1-x}\text{Co}_x)_{11.9}\text{Si}_{1.1}$  [44], these perovskite manganites are easy to manufacture and exhibit higher A-or B-site doping. Consequently, a large magnetic entropy change can be tuned from low temperature to near or above room temperature which is beneficial for operating magnetic refrigeration at various temperature ranges.

On the other hand, the specific heat can be calculated from the field dependence of the external magnetic entropy from zero to  $\mu_0 H_{\max}$  by the following equation: [51, 52]:

$$\Delta C_p(T, \mu_0 H) = C_p(T, \mu_0 H) - C_p(T, 0) = -T \frac{\partial (\Delta S_M(T, \mu_0 H))}{\partial T} \quad (3)$$

From this formula,  $\Delta C_p(T, \mu_0 H)$  of  $\text{La}_{0.6}\text{Pr}_{0.1}\text{Sr}_{0.3}\text{Mn}_{1-x}\text{Ru}_x\text{O}_3$  for ( $x=0.05$ ) sample versus temperature at different magnetic fields is shown in **Fig. 7**. The value of  $\Delta C_p$  suddenly changes from positive to negative around Curie temperature ( $T_C$ ) and rapidly decreases with decreasing temperature.

For practical applications, not only the high value of  $\Delta S_M$ . but also the temperature range over which it remains large is important. The relative cooling power (RCP), defined as the product of peak value of  $\Delta S_M$  and full width at half maximum (FWHM) of  $\Delta S_M$  in the corresponding temperature scale ( $RCP = \Delta S_M \times \partial T_{FWHM}$ ), is a measure of the quantity of heat transferred by the magnetic refrigerant between hot and cold sinks. We found that  $RCP = 227.445$  J/Kg,  $214.148$  J/Kg and  $188.684$  J/Kg. for  $x=0.00$ ,  $0.05$  and  $0.15$  respectively. These values are higher than those of  $\text{La}_{0.67}\text{Ba}_{0.33}\text{MnO}_3$  ( $RCP = 161$  J/Kg at  $T=T_C$ ) [53]. Since the RCP factor represents a good way for comparing magnetocaloric materials, our compounds can be considered as potential candidates thanks to their high RCP values compared with available refrigerant materials [41, 43].

We can use  $\Delta S_M^{\max}$  and  $\mu_0 H$  to confirm that our materials exhibit a second order transition [54, 55]. The magnetic materials with a second order transition generally obey  $\Delta S_M^{\max} = -k M_S(0) h^{2/3} - S(0,0)$ , where  $h$  is the reduced field just around  $T_C$  [ $h = (\mu_0 \mu_B H) / (k_B T_C)$ ],  $k$  is a constant,  $M_S(0)$  is the saturation magnetization at low temperatures and  $S(0,0)$  is the reference parameter, which may not be equal to zero [55]. Fig. 8 shows the linear dependence of  $\Delta S_M^{\max}$  versus  $h^{2/3}$  which implies the second order transition in  $\text{La}_{0.6}\text{Pr}_{0.1}\text{Sr}_{0.3}\text{Mn}_{1-x}\text{Ru}_x\text{O}_3$  for ( $x=0.00, 0.05$  and  $0.15$ ). The fact that  $\Delta S_M^{\max}$  is estimated at  $T_C$  and in fields larger than the critical field required for the metamagnetic transition justifies the conclusion about the second order transition.

A phenomenological universal curve for the field dependence of  $\Delta S_M$  has recently been proposed [56], being the theoretical justification for its existence based on scaling relations [57]. Its phenomenological construction is based on the assumption that if such a universal curve exists, the equivalent points belonging to several  $\Delta S_M(T)$  curves measured up to different maximum applied fields should collapse onto the same point of the universal curve. Therefore, the main aspect of constructing the universal scaling curve has been the selection of the equivalent points of the experimental curves. For this purpose, the peak entropy change  $|\Delta S_M^{\max}|$  is taken as a reference. It was assumed that all points that are at the same level with respect to  $|\Delta S_M^{\max}|$  should be in an equivalent state.

This phenomenological universal curve can be constructed by normalizing all  $\Delta S_M(T)$  curves by using their respective maximum value  $\Delta S_M^{\max}$ , namely,  $\Delta S' = \Delta S_M(T) / \Delta S_M^{\max}$  and by rescaling the temperature axis below and above  $T_C$ , as defined in (Eq.4) with an imposed constraint that the position of two additional reference points in the curve corresponds to  $\theta = \pm 1$ :

$$\begin{cases} \theta = (T_C - T) / (T_{r1} - T_C), T \leq T_C \\ \theta = (T - T_C) / (T_{r2} - T_C), T > T_C \end{cases} \quad (\text{Eq.4})$$

Where  $T_{r1}$  and  $T_{r2}$  are the temperatures of the two reference points that were selected as those corresponding to  $0.5 \Delta S_M^{\max}$ . This procedure has been successfully applied to different families of soft magnetic amorphous alloys and lanthanide based crystalline

materials [58-60]. The phenomenological construction of the universal curve for the studied  $\text{La}_{0.6}\text{Pr}_{0.1}\text{Sr}_{0.3}\text{Mn}_{0.95}\text{Ru}_{0.05}\text{O}_3$  manganite is reported in **Fig. 9**.

It can be clearly seen that the experimental points of the samples distribute on one master curve of the magnetic entropy change (ranging from 1T up to 5T), demonstrating the predictions of master curve behavior for different magnetic fields of the same sample. This universal curve can be particularly helpful for studying the order of phase transition and the refrigeration capacity of similar materials, such as manganite series with the same universality class [61].

### 3.4. Correlation between critical exponents and magnetocaloric effect

Numerous works have focused on the dependence of the magnetic entropy change ( $\Delta S_M$ ) of manganites at the FM-PM transition on  $T_C$ . According to Oesterreicher et al. [62], the magnetic field dependence on the magnetic entropy change  $\Delta S_M$  at a temperature  $T$  for materials obeying a second-order phase transition follows an exponent power law of the type  $\Delta S_M = b(\mu_0 H)^n$  [63]:

$$n = \frac{d \ln \Delta S_M}{d \ln \mu_0 H} = - \frac{\mu_0 H}{\Delta S_M} \left( \frac{\partial M}{\partial T} \right)_{\mu_0 H} \quad (5)$$

where  $b$  is a constant and the exponent  $n$  depends on the values of field and temperature. By fitting the data of  $\Delta S_M$  versus  $\mu_0 H$  to **Eq.4**, we obtained the value of  $n$  as a function of temperature at different magnetic fields for example  $x=0.05$ , as depicted in **Fig.10**. From this figure, the exponent  $n$  is close to 1 in the FM regime and increases to 2 in the PM regime. The exponent  $n$  exhibits a moderate increase with decreasing temperature and takes extreme values around Curie temperature of the existing phase, then sharply increases with increasing temperature. In a mean field approach, the value of  $n$  at Curie temperature is predicted to be  $2/3$  [55]. It is well known in manganites that the exponent is roughly field independent and approaches approximate values of 1 and 2, far below and above the transition temperature respectively [64]. Then the values of  $n$  around  $T_C$  are 0.561, 0.584 and 0.613 for  $x=0.00$ , 0.05 and 0.15 respectively, which confirms not only the invalidity of the mean field model in the description of our materials at near the transition temperature for our samples but also the possibility of 3D Ising model and 3D Heisenberg model

to describe our material. These values are similar to those obtained for soft magnetic materials containing rare earth metals [65-67].

The field dependence of RCP, for our samples is also analyzed. It can be expressed as a power law by taking account of the field dependence of entropy change  $\Delta S_M$  and reference temperature into consideration [57].

$$RCP \propto \mu_0 H^{1+\frac{1}{\delta}} \quad (6)$$

Where  $\delta$  is the critical exponent of the magnetic transition. Field dependence of RCP is displayed in **Fig.11** for  $x = 0.05$ . The obtained values of  $\delta$  are 3.2 (3), 3.34 (2), and 2.82 (4) for  $x = 0.00, 0.05$  and  $0.15$ , respectively. In the particular case of  $T = T_C$  or at the temperature when the entropy is maximal, the exponent ( $n$ ) becomes an independent field [68]. In this case,

$$n(T_C) = 1 + \frac{\beta - 1}{\beta + \gamma} \quad (7)$$

Where  $\beta$  and  $\gamma$  are the critical exponents [69]. With  $\beta \delta = (\beta + \gamma)$  [69], the relation (Eq.7) can be written as:

$$n(T_C) = 1 + \frac{1}{\delta} \left(1 - \frac{1}{\beta}\right) \quad (8)$$

From the values of  $n$  and  $\delta$ , the critical parameters  $\beta$  and  $\gamma$  are deduced for each compound using (Eq.7) and (Eq.8) (Table 3).

#### 4. Conclusion:

In conclusion, we have reported detailed investigations of Morphological, magnetic and magnetocaloric properties of  $\text{La}_{0.6}\text{Pr}_{0.1}\text{Sr}_{0.3}\text{Mn}_{1-x}\text{Ru}_x\text{O}_3$  for ( $x=0.00, 0.05$  and  $0.15$ ). The samples were prepared by the standard ceramic process.  $T_C$  decreases slowly by substituting Ru for Mn. Moreover, there is cluster spin state in all investigated samples at low temperatures. We also found that the entropy change and the relative cooling power during the transition phase are reduced with the increase in Ru. These observations indicate that the existence of Ru has the effect of weakening ferromagnetism in LPSMRO perovskite.

#### References:

- <sup>1</sup> R. Thaljaoui, W. Boujelben, M. Pȩkała, K. Pȩkała, J. Antonowicz, J.-F. Fagnard, Ph. Vanderbemden, S. Dąbrowska, J. Mucha. *J. Alloys Comp.* 2014, 611, 427.
- <sup>2</sup> S. Jin, T. H. Tiefel, M. McCormack, R. A. Fastnacht, R. Ramesh, and L. H. Chen, *Science*. 1994, 264, 413.
- <sup>3</sup> K. Khazeni, Y. X. Jia, L. Lu, V. H. Crespi, M. L. Cohen, and A. Zettl, *Phys. Rev. Lett.* 1996, **76**, 295.
- <sup>4</sup> S.K.Giri, Papri Dasgupta, A. Poddar, A.K. Nigam, T.K. Nath. *J. Alloys Compd.* 2014, 582, 609-616.
- <sup>5</sup> A. M. Balagurov, S. N. Bushmeleva, V. Yu. Pomjakushin, D. V. Sheptyakov, V. A. Amelichev, O. Yu. Gorbenko, A. R. Kaul, E. A. Gan'shina, and N. B. Perkins, *Phys. Rev. B*, 2004, **70** 014427.
- <sup>6</sup> E. Granado, Q. Huang, J. W. Lynn, J. Gopalakrishnan, and K. Ramesha. *Phys. Rev. B* . 2004,**70**. 214416.
- <sup>7</sup> M.H. Phan, S.C. Yu, *J. Magn. Mater.* .2004.308, 325.
- <sup>8</sup> I. Dincer, E. Yüzüak, G. Durak, Y. Elerman. *J. Alloys Compd.* 2014. 588.332.
- <sup>9</sup> Yikum Zhang, Baijun Yang. *J. Alloys Compd.* 2014, 610, 540.
- <sup>10</sup> X. Bohigas, J. Tejada, E. Del Barco, X.X. Zhang, M. Sales, *Appl. Phys. Lett.* 1998,73, 390.
- <sup>11</sup> E. Bruck, *J. Phys. D: Appl. Phys.* 2005,38, 381.
- <sup>12</sup> H. Takeya, V.K. Pecharsky, K.A. Gschneidner Jr., J.O. Morman, *Appl. Phys. Lett.* 1994,64, 2739.
- <sup>13</sup> Saoussen Mahjoub, Mohamed Baazaoui, Rafik M'nassri, Hedi Rahmouni, Nassira Chniba Boudjada, Mohamed Oumezzine . *J. Alloys Comp.* 2014, 608 191.
- <sup>14</sup> B. Podmiljsak, J.-H. Kim, P.J. McGuinness, S. Kobe. *J. alloys Compd.* 2014, 608, 29.
- <sup>15</sup> J.R. Sun, G.H. RAO, B.G. Shen and H.K. Wong, *Appl. Phys. Lett.* 1988. 73, 2998
- <sup>16</sup> K. Ghosh, S. B. Ogale, R. Ramesh, R. L. Greene, T. Venkatesan, K. M. Gapchup, R. Bathe, and S. I. Patil, *Phys. Rev. B*, 1999, **59**, 533-537.
- <sup>17</sup> Y. Huang, C. Liao, Z. Wang, X. Li, C. Yan, J. Sun, and B. Shen, *Phys. Rev. B*, 2002, **65** , 184423.

- <sup>18</sup> Elaa Oumezzine, Sobhi Hcini, El-Kebir Hlil, Essebti Dhahri, Mohamed Oumezzine. *J. alloys Compd.* 2014, 615, 553.
- <sup>19</sup> C. Martin, A. Maignan, M. Hervieu, C. Autret, B. Raveau, and D. I. Khomskii, *Phys. Rev. B*, 2001, **63**, 174402.
- <sup>20</sup> L. Pi, S. Hebert, C. Martin, A. Maignan, and B. Raveau, *Phys. Rev. B*. 2003, **67**, 024430.
- <sup>21</sup> Brajendra Singh, Ranjan K. Sahu, S. Sundar Manoharan, K. Dorr, and K.-H. Muller, *J. Magn. Magn. Mater.* 2004, 270, 358.
- <sup>22</sup> S. S. Manoharan, H. L. Ju, and K. M. Krishnan, *J. Appl. Phys.* 1998, 83, 7183-7185.
- <sup>23</sup> K. S. Ranjan, Q. Mohammad, L. R. Manju, S. S. Manoharan, and A. K. Nigam, *Appl. Phys. Lett.* 2002, 80, 88.
- <sup>24</sup> B. Raveau, A. Maignan, C. Martin, R. Mahendiran, M. Hervieu, *J. Sol Sta Chem.* 2000, 151, 330.
- <sup>25</sup> Biao Hu, Gregory T. McCandless, V. O. Garlea, S. Stadler, Yimin Xiong, Julia Y. Chan, E. W. Plummer, and R. Jin, *Phys Rev B*, 2011, 84, 174411.
- <sup>26</sup> Tae Hwan Kim, M. Angst, B. Hu, R. Jin, X.G. Zhang, J. F. Wendelken, E. W. Plummer, and AnPing Li, *Proceedings Nat Aca Sci*, 2010, 107, 52725275.
- <sup>27</sup> Haizhong Guo, Yi Li, Darwin Urbina, Biao Hu, Rongying Jin, Tijiang Liu, David Fobes, Zhiqiang Mao, E. W. Plummer, and Jiandi Zhang, *Phys Rev B*, 2010, 81, 155121.
- <sup>28</sup> Guorong Li, Qing Li, Minghu Pan, Biao Hu, Chen Chen, Jing Teng, Zhenyu Diao, Jiandi Zhang, Rongying Jin, and E. W. Plummer, *Sci Rep* .2013, 3, 2882.
- <sup>29</sup> Dalgis Mesa, F. Ye, S. Chi, J. A. FernandezBaca, W. Tian, Biao Hu, R. Jin, E. W. Plummer and J. Zhang, *Phys Rev B(R)* .2012, 85, 180410.
- <sup>30</sup> A. Tiwari, J. Narayan, N. Sudhakar, K.P. Rajeev. *J. Sol Sta Com.* 2004, 132,635.
- <sup>31</sup> L. M. Wang, Jian-Hong Lai, and Jyh-Iuan Wu. *J. App Phys* 2007, 102, 023915.
- <sup>32</sup> R. Cherif, E.K.Hlil, M.Ellouze, F.Elhalouani, S.Obbade *J. Sol Sta Chem* 2014, 215, 271.
- <sup>33</sup> Seshu B. Desu, *J. Am. Ceram. Soc.* 1990, 73, 3407.
- <sup>34</sup> S. Zemni, A. Gasmi, M. Boudard, M. Oumezzine, *J. Mat Sci and Eng B*, 2007,144, 117.

- <sup>35</sup> Yue Ying, Jiyu Fan, Li Pi, Zhe Qu, Wenqin Wang, Bo Hong, Shun Tan, and Yuheng Zhang. *Phys. Rev. B.* 2006, **74**, 144433.
- <sup>36</sup> S. Hcini, S. Zemni, A. Triki, H. Rahmouni, M. Boudard. *J. Alloys Comp.* 2011, 509, 1394.
- <sup>37</sup> J. A. HODGES et F. CHANTEREAU. *J. PHYQ.* 1973, 623.
- <sup>38</sup> A. Buteraa, M. Vasquez Mansilla, A. Fainsteina, G.V.M. Williams. *Phys B* 2002, 320, 316.
- <sup>39</sup> Sagar E. Shirsath, S.S. Jadhav, B.G. Toksha, S.M. Patange, K.M. Jadhav, *J. Appl. Phys.* 2011, 110, 013914.
- <sup>40</sup> R. Cherif, E.K.Hlil, M.Ellouze, F.Elhalouani, S.Obbade. *J. Sol Sta Chem.* 2014, 215, 271.
- <sup>41</sup> B.K. Banerjee, *Phys. Lett.* 1964, 12, 16.
- <sup>42</sup> M.Pekala, V. Drozd, *J. Non-Cryst. Solids.* 2008, 354, 5308.
- <sup>43</sup> S. Ghodhbane, A. Dhahri, N. Dhahri, E.K. Hlil, J. Dhahri. *J. Alloys Comp.* 2013, 550, 358.
- <sup>44</sup> Hu Feng-Xia, Qian Xiao-Ling, Wang Guang-Jun, Sun Ji-Rong, Shen Bao-Gen, Cheng Zhao-Hua and Gao Ju. *Chin Phys.* 2005, 14, 2329.
- <sup>45</sup> A. Selmi, R. M'nassri, W. Cheikhrouhou-Koubaa, N. Chniba Boudjada, A. Cheikhrouhou. *J. Alloys Comp.* 2015, 619, 627.
- <sup>46</sup> O. Tegus, E. Brück, K.H.J. Buschow, F.R. de Boer, *Nature.* 2002, 415, 150.
- <sup>47</sup> N. Zaidi, S.Mnefgui, A.Dhahri, J.Dhahri, E.K.Hlil. *Phys B.* 2014, 450, 155.
- <sup>48</sup> V. Franco, C.F. Conde, L.F.Kiss. *J. Appl.Phys.letl.* 2007, 90, 052509.
- <sup>49</sup> D.T. Morelli, A.M. Mance, J.V. Mantese, A.L. Micheli, *J. Appl. Phys.* 1996, 79, 373.
- <sup>50</sup> S. Zemni, M. Baazaoui, Ja. Dhahri, H. Vincent, M. Oumezzine. *J. Mater. Lett.* 2009, 63, 489.
- <sup>51</sup> R. M'nassri, A. Cheikhrouhou. *J. Sup Nov Magn*, 2014, 27, 1059.
- <sup>52</sup> R. M'nassri, A. Cheikhrouhou. *J. Kor Phys Soc*, 2014, 64, 879.885.

- <sup>53</sup> M. Oumezzine, S. Zemni, O. Pena, J. Alloys Compd. 2010,508, 292.
- <sup>54</sup> Dong Q. Y. Zhang H. W. Shen J. L, Sun J. R and Shen B.G. J. Magn. Mater. 2007,319, 56.
- <sup>55</sup> Franco V, Conde A, Pecharsky V.K and Gschneidner K. A, J. Euro Phys. Lett. 2007,79, 47009.
- <sup>56</sup> V. Franco, J.S. Blázquez, A. Conde, Appl. Phys. Lett. 2006, 89, 222512 .
- <sup>57</sup> V. Franco, A. Conde, Int. J. Refrig. 2010, 33, 465.
- <sup>58</sup> R. M'nassri, N. Chniba Boudjada, A. Cheikhrouhou. J. Alloys Compd 2015, 626, 20.
- <sup>59</sup> Yantao Su, Yu Sui, J.-G. Cheng, J.-S. Zhou, Xianjie Wang, Yang Wang, and J. B. Goodenough. Phys Rev B ,2013, **87**, 195102.
- <sup>60</sup> R. M'nassri. J Supe Nov Magn ,2014, 27,1787.
- <sup>61</sup> V. Franco, J.S.Blázquez, A. A.Conde. J.Appl.Phys. , 2008, 103, 07B316.
- <sup>62</sup> H. Oesterreicher, F.T.Parker. J. Appl. Phys. 1984,55 , 4334.
- <sup>63</sup> T.D. Shen, R.B.Schwarz, J.Y. Coulter, J.D.Thompson. J.Appl. Phys.2002,91, 5240.
- <sup>64</sup> M.Pekala, J. Appl. Phys.2010, 108, 113913.
- <sup>65</sup> V. Franco,C.F.Conde,J.S.Blazquez,A.Conde,P.Svec,D.Janičkovic, L.F.Kiss, J. Appl.Phys.2007,101, 093903.
- <sup>66</sup> P. Nisha, S. Savitha Pillai, M. Raama Varma, K.G. Suresh. J. Solid State Sci.2012 14 , 40e47.
- <sup>67</sup> K.h.K. Aliev, I.K. Karnilov, A.M. Ormarov, Sov. Phys. JETP ,1988,67, 2262.
- <sup>68</sup> V. Franco, A. Conde, M.D. Kuz'min, J.M. Romero-Enrique, J. Appl. Phys. 2009, 105, 917.
- <sup>69</sup> B. Widom, J. Chem. Phys. 1965, 43, 3898

**Tables legends:**

**Table 1:** Maximum entropy change  $|\Delta S_M^{\max}|$  and relative cooling power (RCP), occurring at the Curie temperature ( $T_C$ ) and under magnetic field 5T for  $\text{La}_{0.6}\text{Pr}_{0.1}\text{Sr}_{0.3}\text{Mn}_{1-x}\text{Ru}_x\text{O}_3$  for ( $x=0.00, 0.05$  and  $0.15$ ) compounds, compared to several materials considered for magnetic refrigeration.

**Table 2:** Table 3: Magnetic parameters deduced from magnetization such as the effective moment (experimental)  $\mu_{\text{eff}}^{\text{exp}}$ , effective moment (theoretical)  $\mu_{\text{eff}}^{\text{cal}}$ , remanence magnetization  $M_r$  (emu/g), saturation magnetization (Ms), the coercive field  $\mu_0 H_C$  (T) and remanence ratio  $R=(M_r/M_s)$  of the system  $\text{La}_{0.6}\text{Pr}_{0.1}\text{Sr}_{0.3}\text{Mn}_{1-x}\text{Ru}_x\text{O}_3$  for ( $x=0.00, 0.05$  and  $0.15$ ) compounds.

**Tableau .3:** Critical  $\beta$  and  $\gamma$  parameters calculated from  $n$  and  $\delta$

| <b>Composition</b>   | <b>T<sub>C</sub> (K)</b> | <b>μ<sub>0</sub>ΔH<br/>(T)</b> | <b> ΔS<sub>M</sub><sup>max</sup> <br/>(J/Kg K)</b> | <b>RCP<br/>(J/Kg)</b> | <b>References</b> |
|--|--------------------------|--------------------------------|--|-----------------------|-------------------|
| La <sub>0.6</sub> Pr <sub>0.1</sub> Sr <sub>0.3</sub> MnO <sub>3</sub>                                     | 360                      | 5                              | 3.32(1)  | 227.44(3)             | <b>Our work</b>   |
| La <sub>0.6</sub> Pr <sub>0.1</sub> Sr <sub>0.3</sub> Mn <sub>0.95</sub> Ru <sub>0.05</sub> O <sub>3</sub> | 350                      | 5                              | 3.11(2)  | 214.14(1)             | <b>Our work</b>   |
| La <sub>0.6</sub> Pr <sub>0.1</sub> Sr <sub>0.3</sub> Mn <sub>0.85</sub> Ru <sub>0.15</sub> O <sub>3</sub> | 344                      | 5                              | 2.57(2)  | 188.68(2)             | <b>Our work</b>   |
| La <sub>0.52</sub> Dy <sub>0.15</sub> Pb <sub>0.33</sub> MnO <sub>3</sub>                                  | 290                      | 5                              | 3.51   | 246                   | [41]              |
| Gd <sub>5</sub> (Si <sub>2</sub> Ge <sub>2</sub> )   | 275                      | 5                              | 18.5   | 535                   | [42]              |
| La <sub>0.8</sub> Ba <sub>0.2</sub> Mn <sub>0.1</sub> Fe <sub>0.1</sub> O <sub>3</sub>                     | 193                      | 5                              | 2.62   | 211                   | [43]              |
| La (Fe <sub>0.96</sub> Co <sub>0.04</sub> ) <sub>11.9</sub> Si <sub>1.1</sub>                              | 243                      | 5                              | 22.5   | -                     | [44]              |
| La (Fe <sub>0.94</sub> Co <sub>0.06</sub> ) <sub>11.9</sub> Si <sub>1.1</sub>                              | 274                      | 5                              | 20   | -                     | [44]              |
| Pr <sub>0.7</sub> Ca <sub>0.3</sub> Mn <sub>0.95</sub> Fe <sub>0.05</sub> O <sub>3</sub>                   | 89.95                    | 5                              | 2.39   | 337.4                 | [45]              |
| Pr <sub>0.7</sub> Ca <sub>0.3</sub> Mn <sub>0.95</sub> Co <sub>0.05</sub> O <sub>3</sub>                   | 104.97                   | 5                              | 2.96   | 378.2                 | [45]              |
| Pr <sub>0.7</sub> Ca <sub>0.3</sub> Mn <sub>0.95</sub> Ni <sub>0.05</sub> O <sub>3</sub>                   | 109.97                   | 5                              | 3.1  | 352.2                 | [45]              |
| Pr <sub>0.7</sub> Ca <sub>0.3</sub> Mn <sub>0.95</sub> Cr <sub>0.05</sub> O <sub>3</sub>                   | 139.7                    | 5                              | 2.92   | 405.72                | [45]              |
| Gd   | 350                      | 5                              | 2  | -                     | [46]              |
| La <sub>0.52</sub> Dy <sub>0.15</sub> Pb <sub>0.33</sub> MnO <sub>3</sub>                                  | 290                      | 5                              | 3.51   | 246                   | [47]              |
| La <sub>0.47</sub> Dy <sub>0.2</sub> Pb <sub>0.33</sub> MnO <sub>3</sub>                                   | 277                      | 5                              | 2.3  | 215                   | [47]              |
| La <sub>0.67</sub> Sr <sub>0.33</sub> MnO <sub>3</sub>   | 348                      | 5                              | 1.69   | 211                   | [48]              |
| La <sub>0.67</sub> Ba <sub>0.33</sub> MnO <sub>3</sub>   | 292                      | 5                              | 1.48   | 161                   | [49]              |
| La <sub>0.7</sub> Pb <sub>0.3</sub> MnO <sub>3</sub>   | 352                      | 5                              | 0.96   | 48                    | [50]              |

Table.1

| <b>samples</b> | $P_{eff}^{exp}$ | $P_{eff}^{cal}$ | $M_r(\text{emu/g})$ | $\mu_0 H_C(\text{T})$ | $M_s(\text{emu/g})$ | $R=(M_r/M_s)\%$ |
|----------------|-----------------|-----------------|---------------------|-----------------------|---------------------|-----------------|
| <b>x=0.00</b>  | 5.76(3)         | 4.75(1)         | 4.60(1)             | $2.6(3)10^{-3}$       | 84,23(1)            | 0.054           |
| <b>x=0.05</b>  | 5.45(4)         | 4.66(2)         | 5.75(2)             | $6.3(2)10^{-3}$       | 80,11(1)            | 0.071           |
| <b>x=0.15</b>  | 4.91(1)         | 4.47(1)         | 18.20(4)            | $2.3(5)10^{-2}$       | 75,07(3)            | 0.240           |

**Table.2**

| <b>samples</b> | <b>n</b> | <b><math>\delta</math></b> | <b><math>\beta</math></b> | <b><math>\gamma</math></b> | <b>T<sub>C</sub> (K)</b> | <b>References</b> |
|----------------|----------|----------------------------|---------------------------|----------------------------|--------------------------|-------------------|
| <b>x=0.00</b>  | 0.561    | 4.98                       | 0.313                     | 1.251                      | 360                      | This work         |
| <b>x=0.05</b>  | 0.584    | 5.02                       | 0.323                     | 1.304                      | 350                      | This work         |
| <b>x=0.15</b>  | 0.613    | 4.85                       | 0.347                     | 1.340                      | 344                      | This work         |

**Tableau 3**

**Figures captions:**

**Fig.1: (a):** Plot of EDX analysis of chemical species, the inset represents the scanning electron micrograph of  $x=0.05$ .

**Fig.2:** Temperature dependences of the zero-field-cooled and field-cooled magnetization for LPSMRO samples under applied magnetic field 0.05 T, the inset show temperature dependent inverse susceptibility  $\chi^{-1}(T)$  curves. **(b):** The hysteresis loops of LPSMRO samples ( $x=0.00$  and  $0.15$ ); the inset shows the fields dependence of the magnetization plots taken at 5K for all the samples in magnetic fields strengths of  $\pm 10$  T.

**Fig.3:** Variation of saturation magnetization ( $M_s$ ) and remanence magnetization ( $M_r$ ) with Ru content.

**Fig.4:** Isothermal magnetization as a function of applied field for  $\text{La}_{0.6}\text{Pr}_{0.1}\text{Sr}_{0.3}\text{Mn}_{1-x}\text{Ru}_x\text{O}_3$  for ( $x=0.00$  and  $0.15$ ) measured in the temperature ranges 299 to 384 K.

**Fig. 5:** the Arrott plots of  $M^2$  vs  $\mu_0 H/M$  at various temperatures for  $\text{La}_{0.6}\text{Pr}_{0.1}\text{Sr}_{0.3}\text{Mn}_{1-x}\text{Ru}_x\text{O}_3$  for ( $x=0.00$  and  $0.15$ ) samples.

**Fig. 6:** Temperature dependence of the magnetic entropy change ( $-\Delta S_M$ ) at different applied magnetic field change interval for  $\text{La}_{0.6}\text{Pr}_{0.1}\text{Sr}_{0.3}\text{Mn}_{1-x}\text{Ru}_x\text{O}_3$  for ( $x=0.00$ ,  $0.05$  and  $0.15$ ) samples.

**Fig.7:** Change of specific heat of the sample as a function of temperature at different magnetic fields for  $x = 0.05$ .

**Fig. 8:** Temperature dependence of magnetic entropy change  $-\Delta_M^{ma}$  versus  $h^{2/3}$  for  $\text{La}_{0.6}\text{Pr}_{0.1}\text{Sr}_{0.3}\text{Mn}_{1-x}\text{Ru}_x\text{O}_3$  for ( $x=0.00$  and  $0.15$ ) samples.

**Fig.9:** The master curve behavior of the curves as a function of the rescaled temperature for different magnetic field ( $\mu_0 H=5, 4, 3, 2$  T) for  $x=0.05$ .

**Fig.10:** Temperature dependence of the local exponent  $n$  for  $x=0.05$  at different magnetic field.

**Fig.11:** Variation of  $\text{Ln}(\text{RCP})$  as function of applied magnetic field for  $x=0.05$  sample. Red line indicates the linear fit for  $d$  calculation.

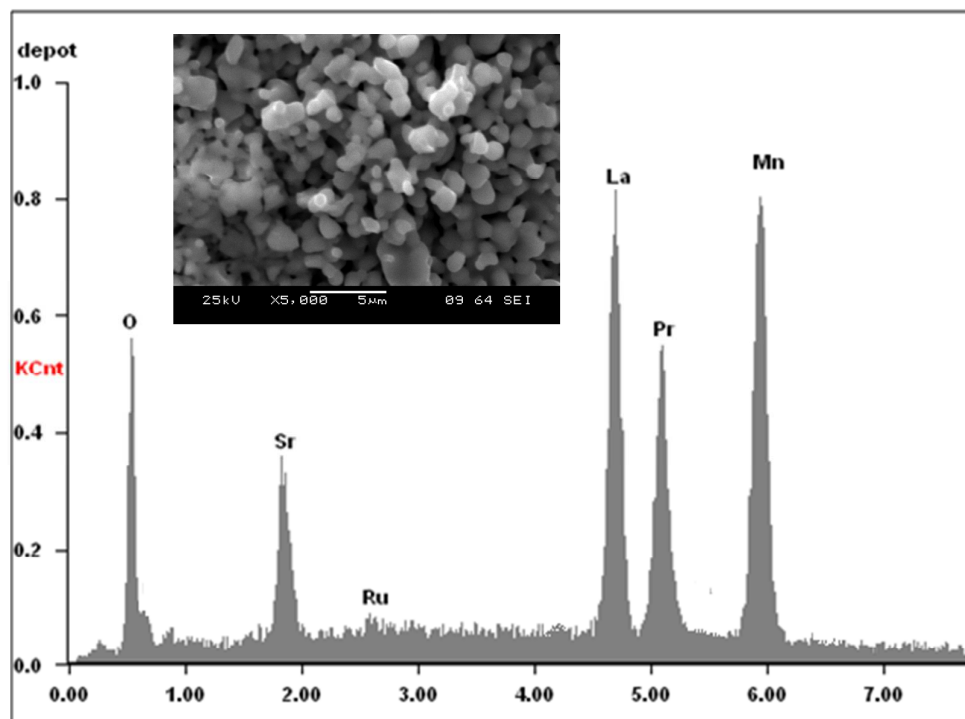


Fig.1

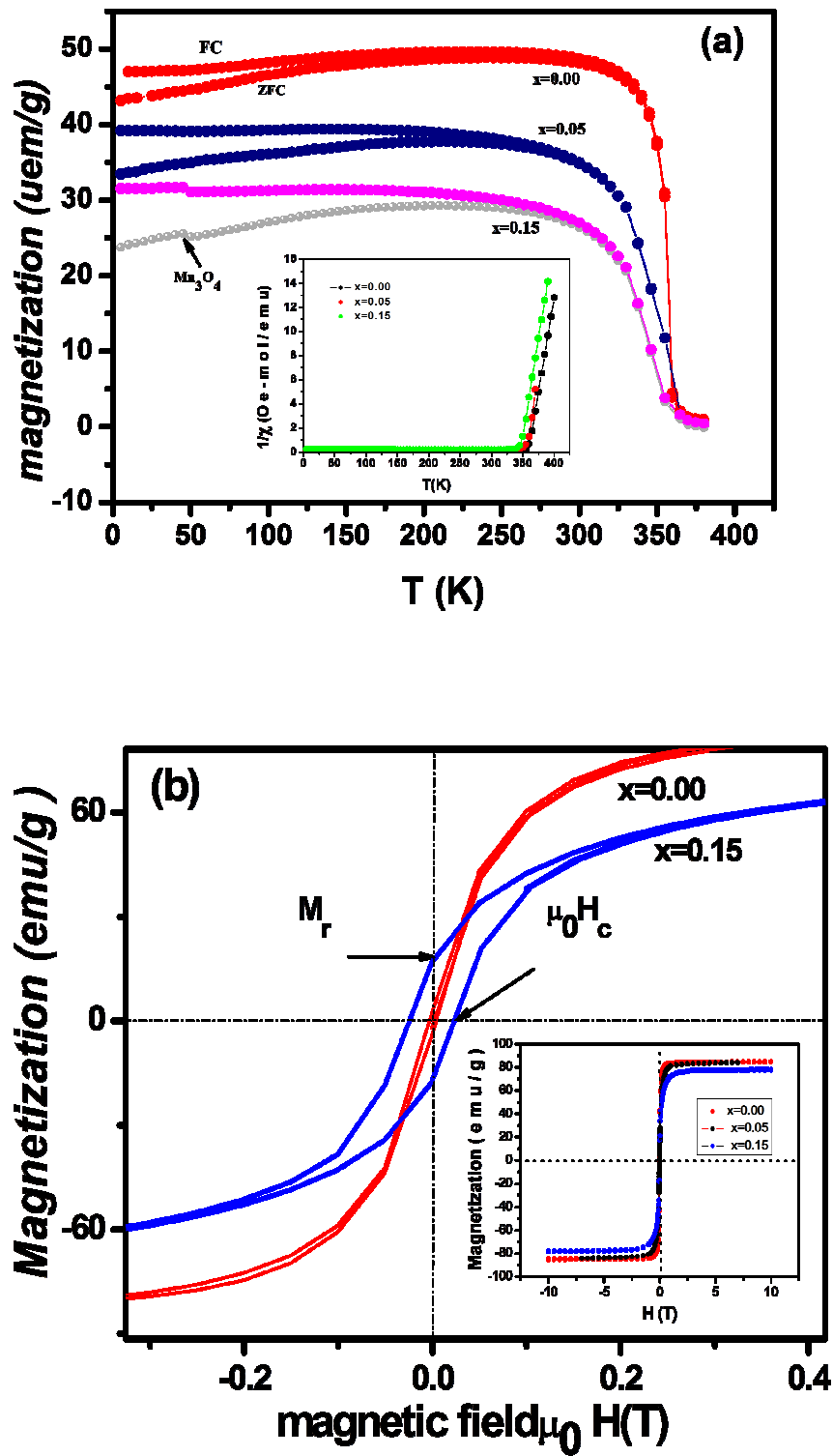


Fig.2

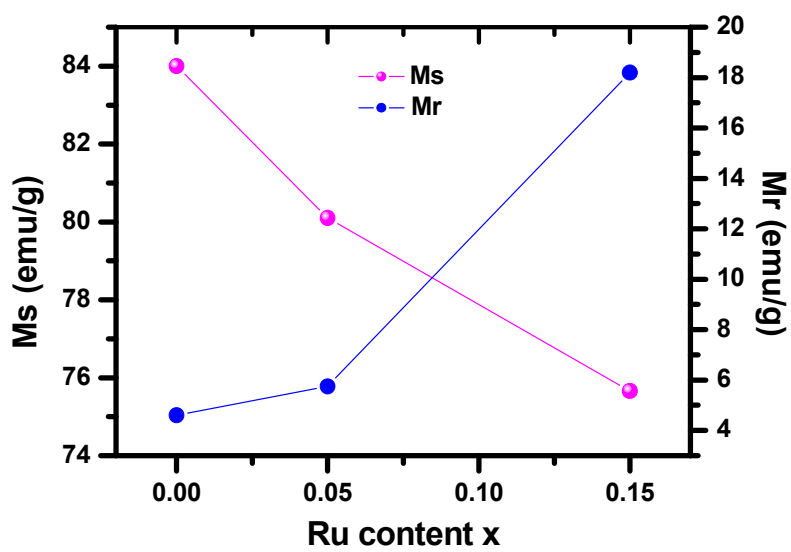


Fig.3

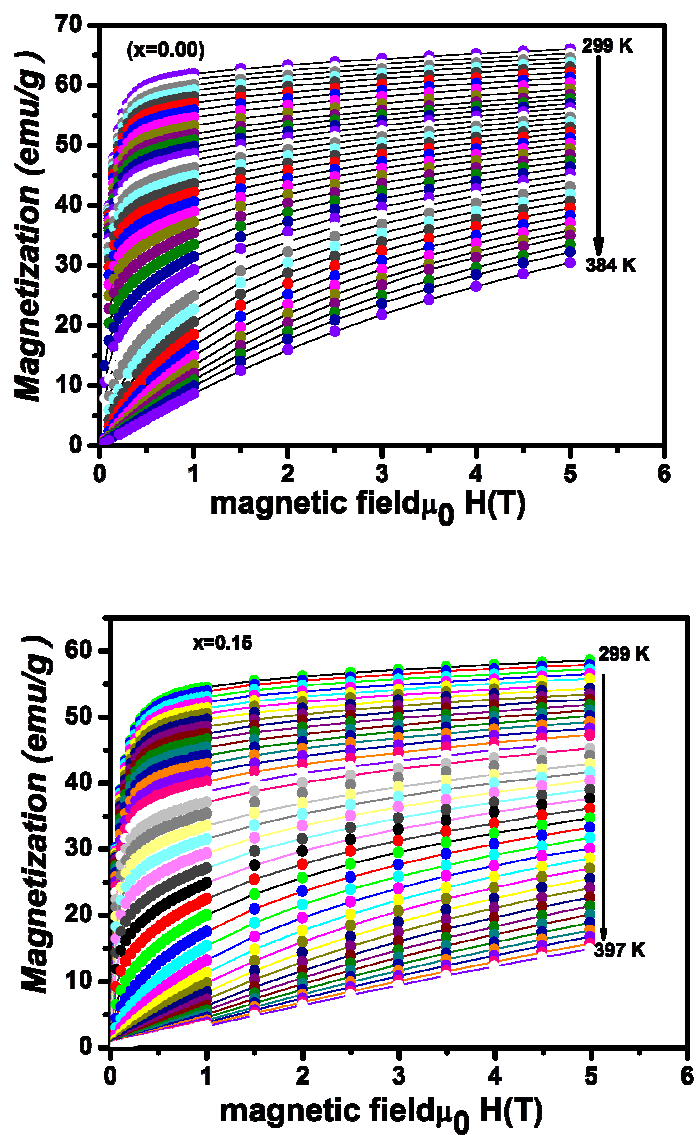


Fig.4

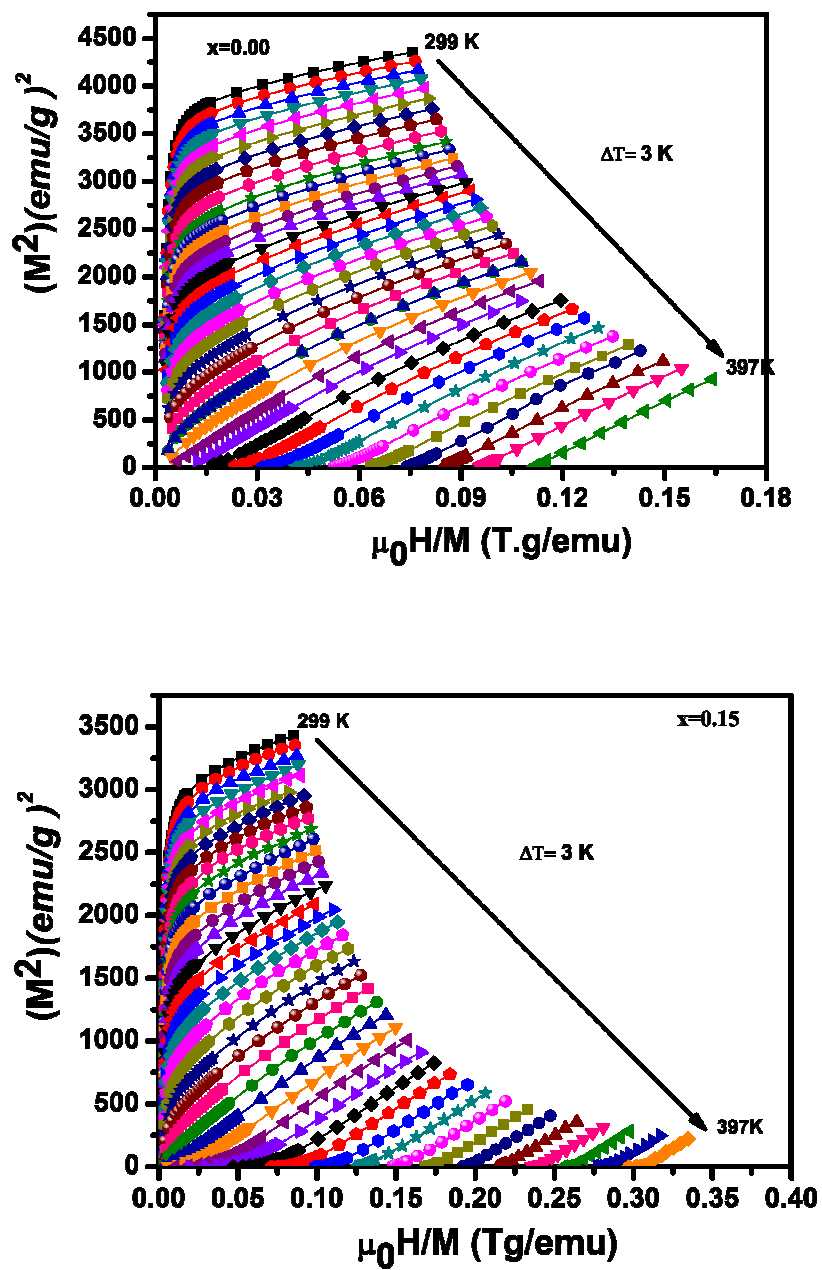


Fig.5

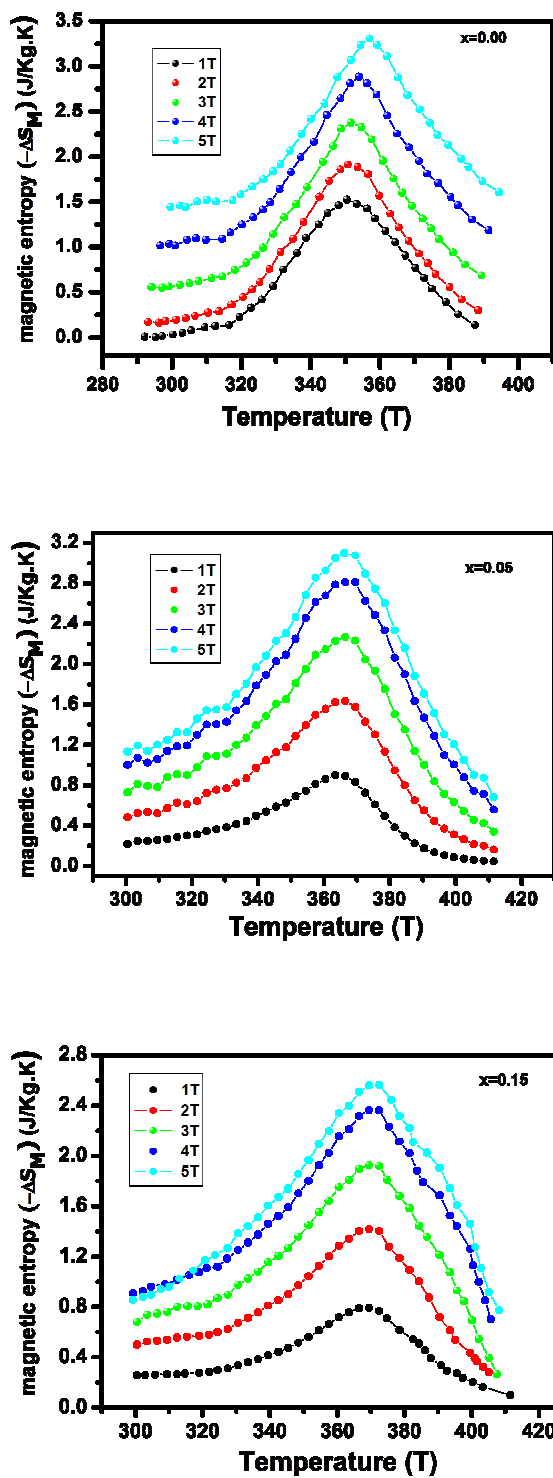


Fig.6

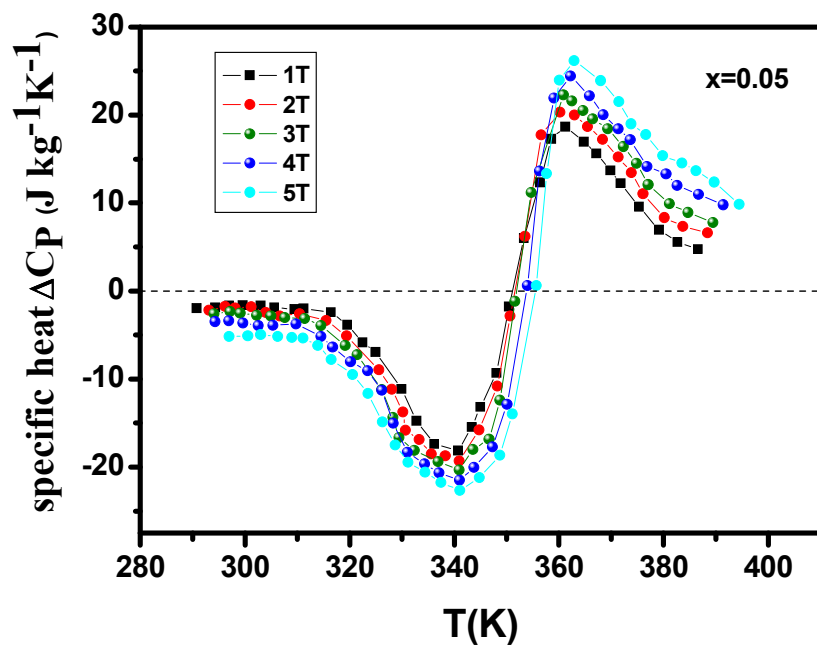


Fig.7

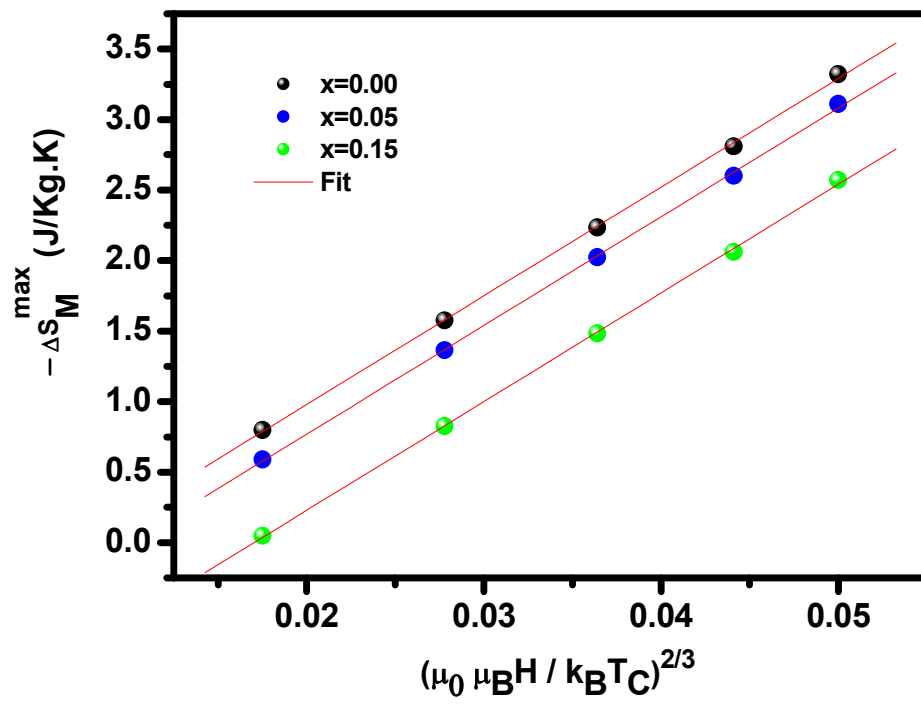


Fig. 8

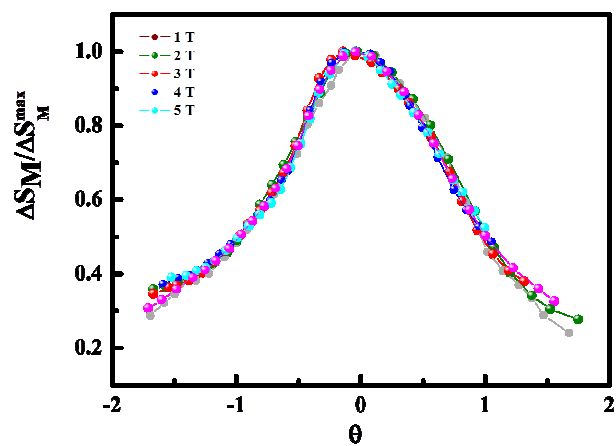


Fig. 9:

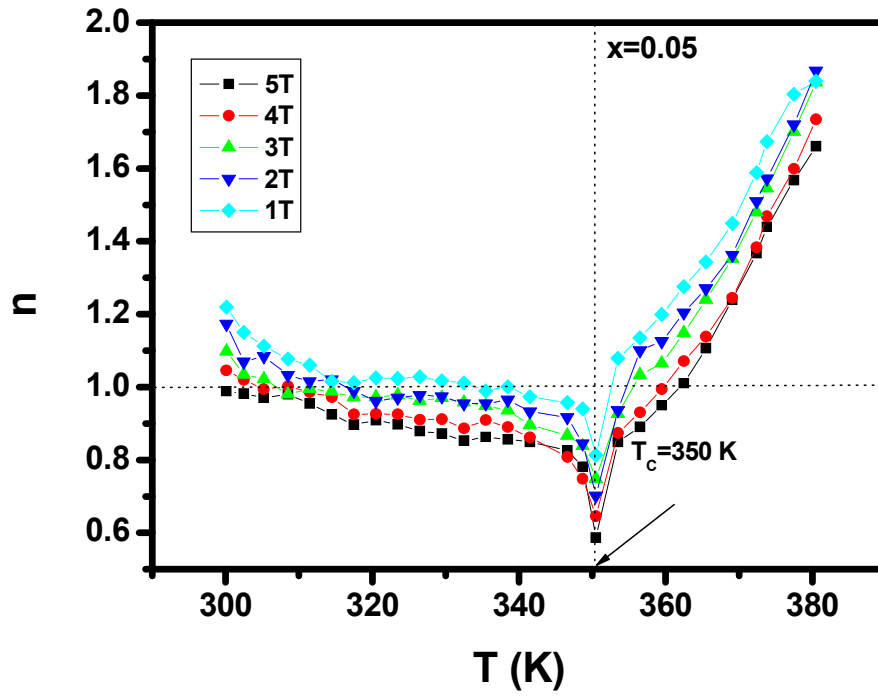


Fig. 10

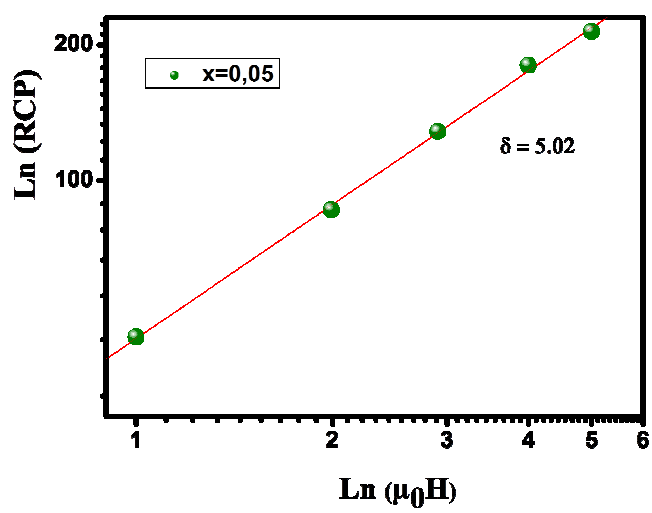


Fig.11